# Penetration depth of photomobilized F atoms in Ar layers from a sandwich experiment

C. Bressler, M. Dickgiesser, and N. Schwentner

Citation: The Journal of Chemical Physics **107**, 10268 (1997); doi: 10.1063/1.474167
View online: http://dx.doi.org/10.1063/1.474167
View Table of Contents: http://scitation.aip.org/content/aip/journal/jcp/107/23?ver=pdfcov
Published by the AIP Publishing

# Penetration depth of photomobilized F atoms in Ar layers from a sandwich experiment

C. Bressler,[a] M. Dickgiesser, and N. Schwentner
*Institut für Experimentalphysik, Freie Universität Berlin, Arnimallee 14, D-14195 Berlin, Germany*

(Received 19 June 1997; accepted 11 September 1997)

The mean value and the distribution of the penetration depth of F atoms is determined from samples composed of three layers with controlled thickness in the monolayer range and with a test of the compactness of the films via the intensity of surface excitons. F atoms with an average kinetic energy of 4.3 eV are generated in the top layer (Ar doped with $F_2$) by photodissociation of $F_2$ with 10.15 eV in a spin forbidden repulsive state. The F atoms are injected into an Ar spacer layer of variable thickness. Those reaching the interface to the Kr bottom layer are monitored via the intensity of the $Kr_2F$ fluorescence at a wavelength of 444 nm, which allows one to discriminate between F in Ar (439 nm), in Kr (453 nm), and at the Kr/Ar (444 nm) interface. The F content at the interface is kept below 1/20th of a monolayer to suppress recombination, and the detection sensitivity is increased to 1/1000th of a monolayer by excitation via Kr exciton energy transfer. The probability for F atoms to penetrate the Ar spacer layer decreases exponentially with increasing thickness down to 10% for a thickness of 23 monolayers, and an average penetration depth of 10 monolayers is derived. These very large penetration depths exceed those of $F^+$ and $F^-$ ions by more than one order of magnitude. They are consistent with those molecular dynamics calculations, which predict a rather rectilinear motion in channels of the Ar lattice. An average length of travel of up to 27 monolayers with a mean-free path (large angle scattering) up to four monolayers is compatible with the results.  [S0021-9606(97)51447-4]

## I. INTRODUCTION

Electronic excitation can lead to local structural rearrangements in a crystal or a liquid, and in this case kinetic energy will be acquired by neighboring particles. Color center formation and light-induced desorption are typical processes resulting from atoms photomobilized in such a way. The distance between the original lattice site of a hot atom and the position where it comes to rest again corresponds to its penetration depth. In general, small values of the order of one lattice constant or less are expected for kinetic energies of some eV, and only more recently, for example, the contribution of subsurface layers to the desorption yields has been considered.[1] The efficiency for photochemical preparation of radicals can critically depend on a large penetration depth of intermediate hot fragments. Concerning the modeling of a condensed phase photoreaction, it would be highly informative if the process can be divided into elementary steps, like photodissociation of a parent molecule providing kinetic energy for the hot fragment, exit of the fragment out of its original cage, transport of the fragment through the lattice to a reactive site, and formation of a new bond. These basic features of condensed phase photochemistry can be studied by means of photodissociation of small molecules, like halogens, $H_2O$, and $H_2S$ in rare gas matrices.[2] Rare gas halides can be stabilized in this way.[3] Photodissociation of $F_2$ in Ar or Ne matrices codoped with Kr or Xe atoms provides high concentrations of about $10^{18}/cm^3$ of XeF and KrF centers. Solid state excimer lasers with about two orders of magnitude higher gain coefficients compared to the gas phase were attained with these crystals in the spectral range from 269 to 560 nm.[4] A large penetration depth of photomobilized F atoms was inferred from the large XeF concentration and the large mean Xe and F separation of 15 lattice constants.[5] The average length of travel of photomobilized F atoms in Ar crystals with excess energies of about 0.74 eV from the $Ar_2F$ radiative decay was studied via the recombination efficiency to $F_2$.[6] Involving assumptions on the statistical distribution of F atoms as well as on branching ratios and on cross sections of the different processes an average length of travel of 7 nm was derived from the concentration dependent decrease in $Ar_2F$ intensity. To obtain further confidence in this large length of travel, the shuttle of F atoms between Xe and Kr in triply doped Ar crystals was investigated.[7] From the Xe, Kr, and $F_2$ concentrations an average length of travel of ten lattice constants (5.3 nm) for the involved kinetic energy of 0.5 eV was estimated.[7] For $F_2$ dissociation in Kr matrices, codoped with Xe atoms of low concentration, the efficiency of XeF formation increased with the kinetic energy of the F atoms. From the dilution of Xe it was concluded that for an excess energy larger than 2.4 eV trajectories with a length of the order of 15 lattice constants (8 nm) occur, whereas the F atoms are trapped close to their original sites for an excess energy of 1.9 eV.[8] These experiments confirm that photomobilized F atoms in Ar and Kr crystals can provide exceptional large lengths of travel that exceed probably even those of potomobilized H atoms[9] with comparable kinetic energies. This property was already exploited for a separation of reactions within the cage from those involving photomobilized or thermally activated F atoms.[10] In this context, it should be

[a]Present address: Molecular Physics Laboratory SRI International, Menlo Park, California 94025.

pointed out that only the migration originating from the kinetic energy acquired in photoexcitation, and not the thermal activated diffusion occurring above 25 K in Ar crystals[11] is considered in this paper.

The above-mentioned experiments are hampered by the necessary averaging over the spatial distribution between F atoms and target atoms. An advanced method that delivers the distribution of the penetration depths together with a reliable quantitative value for its average was presented recently in letter form,[12] and the more complete account of the experiment will be given here. The central idea is to measure the probability of F atoms to cross a spacer layer of defined thickness $d$. F atoms are photomobilized by $F_2$ photodissociation in a $F_2$/Ar top layer, and the probability for penetrating the Ar spacer layer is determined from the amount of F atoms accumulated on the interface with a bottom Kr film. This amount of F atoms follows from the intensity of $Kr_2F$ emission. The layout of this experiment is comparable with that used for measurements of the attenuation of $F^+$ and $F^-$ ion emission. The ion yields are attenuated to less than 1% for a coverage of only three monolayers that was attributed to the closing of channels in the fcc lattice.[1] With regard to this result, it is important to check whether the penetration depth of neutral F atoms is indeed more than one order of magnitude larger.

The migration of F atoms was modeled by classical molecular dynamics calculations[13] of $F_2$ in a cube of 364 Ar atoms. All trajectories ended within the cube for excess energies below 2 eV. For 2 eV, one trajectory and for the highest calculated energy of 2.8 eV four trajectories out of 50 left the cube, which indicates a penetration depth of at least five monolayers for these five trajectories. These long range trajectories show a soft wiggly motion along lattice channels avoiding side steps, and for one trajectory a total length of travel of 3 nm was extrapolated from the loss rate of kinetic energy.[13] The apparent energy dependence and the distribution of penetration depths need to be confirmed experimentally, and kinetic energies of the order of several eV should be employed to provide large average penetration depths. The requirement of sufficient kinetic energy is backed by a modeling of F migration subsequent to the radiative decay of $Ar_2F$ in Ar.[14] According to this calculation, only 2 out of 300 trajectories showed cage exit and no long range migration occurred in marked contrast to the related recombination experiment described above.[6] F atoms offer the advantage of a most facile cage exit for the fragments compared to H, O, and other halogen atoms and a yield of exiting F atoms near unity is observed for excess energies above 2.4 eV.[6–8] For lower energies the orientation of $F_2$ and thus temperature can play a role.[15] The cage exit properties are quite well reproduced by molecular dynamic calculations,[13,16,17] which include the reorientation of the electronic orbital,[17] and by a statistical model.[18]

The preparation of the sandwiches with a check of the compactness of the films is given in Sec. II. In Sec. III we treat the spectroscopic conditions to prepare F atoms with 4.3 eV kinetic energy, the spectroscopic signature of F atoms in the Kr/Ar interface, and the enhancement of sensitivity via Kr excitons. Results for the penetration depths are collected in Sec. IV and discussed in Sec. V.

## II. EXPERIMENT

### A. Spectroscopy

The experiments were conducted at the 3m NIM2 beamline at the synchrotron radiation facility BESSY in Berlin, Germany. Tunable radiation in the range of 30 to 300 nm is obtained by dispersing the synchrotron radiation using the 3m normal incidence primary monochromator.[19] The output of the primary monochromator is focused to a $0.2 \times 0.5\,mm^2$ spot on the sample, providing more than $10^{15}$ photons/s/cm$^2$ around the blaze wavelength of 130 nm within a typical bandwidth of 0.2 nm (1200 lines/mm grating) or 0.4 nm (600 lines/mm grating). Emission spectra in the long-wavelength range from 200 to 1000 nm are recorded using a Czerny–Turner monochromator equipped with one of two 1200 lines/mm gratings blazed at 250 and 500 nm with a typical resolution of 1 nm and a cooled XP2020Q photomultiplier tube or an RCA-C31034 tube. Short-wavelength luminescence in the spectral range from 60 to 300 nm is dispersed with an evacuated Seya-Namioca monochromator (resolution 0.23 nm) and detected with a solar blind photomultiplier (110–300 nm) or a multichannel plate (60–120 nm).

### B. Sample preparation and characterization

A stack of three different rare gas films, as indicated in Fig. 1, was condensed in an ultrahigh vacuum (UHV) on a polished $MgF_2$ substrate that was cooled by a liquid He flow cryostat to adjustable temperatures down to 4 K. The temperature was recorded with a Si diode on the cooling finger and varied with a heater and the He flow. Ar (purity 99.9999%) and Kr (purity 99.998%) from Linde and a mixture of $F_2$/Ar ($F_2$ concentrations of 0.5% and 2%) were stored in three independent UHV reservoirs. The gases were then condensed one by one with a continuous flow from three independent gas deposition tubes (Fig. 1). In this way, mixing prior to and during condensation and also interdiffusion between the different films was avoided. Deposition temperature and deposition rate govern the quality of the films, and a precise choice of the film thicknesses is essential for the penetration depth measurements. The deposition rates were adjusted by sensitive needle valves for each gas to typically 0.1 nm/s. Film thicknesses and deposition rates were determined from the frequency change of a quartz microbalance mounted next to the $MgF_2$ substrate (Fig. 1). The microbalance was calibrated individually for each deposition tube by comparison with oscillations in the reflectivity of the growing films at 200 nm wavelength due to interference effects. The resolution for the frequency reading of 1 Hz leads to an accuracy for the film thicknesses of better than 0.2 nm. Two independent sets of penetration depth measurements with variations in the tube positions and a new calibration cycle were taken to check for systematic errors.

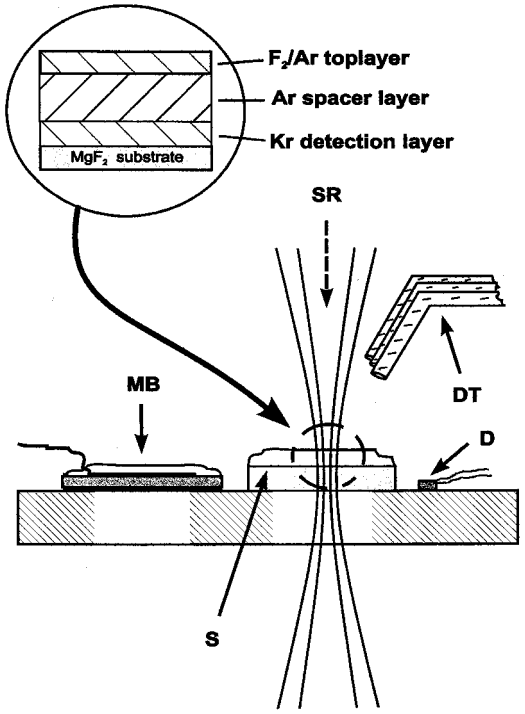


FIG. 1. Samples are grown in on a cold $MgF_2$ substrate ($S$) using three independent deposition tubes (DT) aligned to the synchrotron radiation (SR) focal spot on the substrate. The thickness of the layers is monitored by a quartz microbalance (MB) with an accuracy better than 0.2 nm and the temperature is measured by a Si diode ($D$).

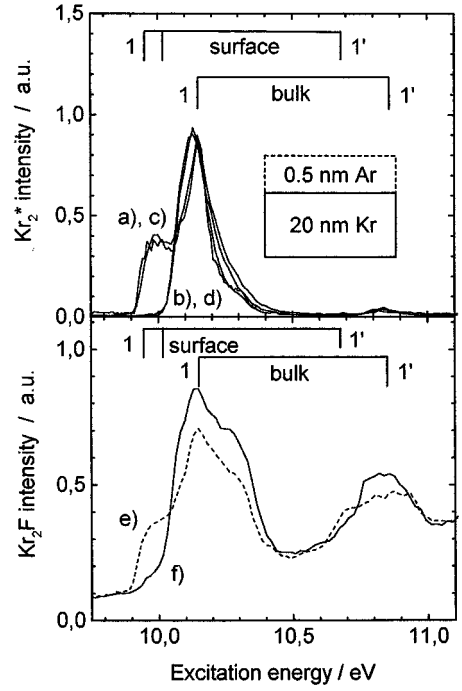


FIG. 2. Top: Luminescence intensity at 147 nm of self-trapped Kr excitons versus excitation energy for different sample conditions: (a) uncovered Kr layer of 20 nm thickness; (b) after additional deposition of 0.5 nm Ar at 4 K; (c) after removing the Ar layer by heating the sample to 40 K; (d) after recovering with 0.5 nm Ar at 4 K. Bottom: $Kr_2F$ luminescence intensity at 444 nm versus excitation energy for two samples composed of 30 nm Kr, 5 nm Ar, and 3 nm $F_2$/Ar (0.5%), and grown at 4 K; (e) the sample grown with a deposition rate of 0.7 nm/s (dashed line); (f) the sample grown with a deposition rate of 0.1 nm/s (solid line). Energies of $n=1$ and $n'=1$ surface and bulk excitons are indicated.

The homogeneity of the thickness of the three films is essential for the method, and especially fluctuations or holes in the Ar spacer layer would lead to an enhanced F transmission and to overestimated penetration depths. The quenching of surface excitons of the Kr substrate was used to determine the optimal conditions, which provide a complete coverage of the substrate by some monolayers of Ar. The spectroscopy of the bulk and surface excitons in absorption and of the trapped excitons observed in the emission of rare gas films is well known.[20] The emission intensity at a wavelength of 147 nm of self-trapped Kr excitons ($Kr_2^*$) versus excitation energy, which is similar to an absorption spectrum, is shown in the region of $n=1$ bulk and surface excitons of Kr for several sample conditions (the top of Fig. 2). The strong contribution between 9.9 and 10 eV in the spectrum of the pure 20 nm thick Kr sample [Fig. 2(a)] demonstrates the presence of and the high sensitivity for the $n=1$ surface excitons. Coverage by a complete monolayer of another rare gas or residual gas is sufficient to suppress the formation of these surface excitons[21] due to the change in boundary conditions. The lack of any contribution from the surface excitons [Fig. 2(b)] after deposition of 0.5 nm ($\approx 2$ monolayers) of Ar at 4 K and with a rate of less than 0.1 nm/s demonstrates that a homogeneous film has been obtained for these preparation conditions that covers the surface without holes. All films used in the following investigation were prepared similarly, and it was checked for each sandwich that the surface excitons had been quenched. The covering experiment is reversible, which excludes falsifying contributions from residual gas. Heating of the covered sample to 40 K removes the top Ar film, and the original spectrum [Fig. 2(c)] with the full surface exciton contribution is restored. Recovering of the sample with 0.5 nm Ar at 4 K leads once more to complete quenching [Fig. 2(d)]. The possibility to grow these homogeneously thick films at the low temperature of 4 K was important since higher temperatures, which lead in general to less defects, would have enhanced interdiffusion and caused calibration problems due to the temperature drift of the microbalance. The necessity of low deposition rates is demonstrated in Fig. 2(e) for which a complete stack was grown at 4 K with a deposition rate of 0.7 nm/s and a composition typical for the F transport experiments. The intensity of the $Kr_2F$ emission is recorded versus excitation energy, which is sensitive to absorption in the Kr substrate near the Kr/Ar interface (see Sec. III) like the trapped exciton emission in Figs. 2(a)–2(d). The strong surface exciton contribution in Fig. 2(e) between 9.9 and 10 eV indicates that quite large holes are present in the layers that reach down to the original surface of the Kr substrate, despite the fact that it was covered by a 5 nm thick Ar layer and topped by a 3 nm thick $F_2$/Ar film. The same experiment with a stack grown with the lower deposition rate of 0.1 nm/s [Fig. 2(f)] shows no surface exciton contribution in accordance with the spectra,

Figs. 2(b) and 2(d), thus confirming that the slowly grown films are homogeneous in thickness and closed. For obtaining flat films it seems that a sufficient number of jumps of the freshly condensed atoms is required in order to find empty places in a monolayer before they are buried by the next atoms. At elevated temperatures this is provided by an enlarged surface mobility while at the low temperature of 4 K a longer time interval resulting from low deposition rates supports the growth of flat films. The stacks are deposited on a cleaned and well polished $MgF_2$ disk to start with a smooth surface. $MgF_2$ is preferable to LiF because it has a weaker background luminescence at 444 nm from color centers.

## III. SPECTROSCOPY

### A. $F_2$ photodissociation

The photodissociation of $F_2$ was carried out with the same wavelength of 122 nm (10.15 eV), which was used for the excitation and detection of the F atoms to allow a continuous monitoring of the growth of the F atom content at the Kr/Ar interface. Absorption spectra from the transmission of about 1 $\mu$m thick Ne and Ar films doped with 0.2% $F_2$ were presented in Figs. 7(a) and 7(b) of Ref. 22. A broad absorption is centered around 11 eV in Ne. It is slightly red shifted in Ar to about 10.7 eV and shows a nearly constant cross section in the region from 10 to 11 eV. The cross sections in these maxima are at least one order of magnitude smaller compared to those transitions to bound states of $F_2$ occurring at energies above 12 eV, as treated in detail in Ref. 22. In Ne the band is situated near the red wing of the $C\ ^1\Sigma_u^+$ absorption and in Ar just below the $n=1$ and $n'=1$ matrix excitons. The similar transition energies in Ne and Ar exclude an assignment to rare gas fluorine charge transfer states. The large width and the absence of any vibrational structure indicate a transition to a repulsive $F_2$ potential surface. All transitions to repulsive states in this energy range are not dipole allowed according to the calculations in Ref. 23, which is in agreement with the observed small cross section. The vertical transition energies of three states with $^{1,3}\Sigma_u^-$ and $^3\Sigma_u^+$ symmetries are situated above 10 eV. The observed bands are attributed to the $2\ ^3\Sigma_u^+ \leftarrow X\ ^1\Sigma_g^+$ transition due to the analogs $Cl_2$ case,[24] and since its calculated transition energy of 10.76 eV[23] is closest to the experimental value. The strength of this spin forbidden transition is perhaps increased compared to the gas phase by an increased mixing with the $C\ ^1\Sigma_u^+$ state, which is red shifted in Ne matrices.[22]

No fluorescence is observed for excitation into these bands in contrast to the transition to bound states[22] that supports once more the assignment to a repulsive state and indicates that nonradiative transitions to lower lying bound states are negligible. Thus, $F_2$ is dissociated by 10.15 eV in the photomobility experiments, and subtracting the ground state binding energy of 1.61 eV[25] leads to an excess energy of 8.5 eV that can be distributed to the two F atoms. A symmetric distribution, like in a free $F_2$ molecule, seems to be favored for the cage exit in the matrix according to the simulations.[13] Thus photomobile F atoms with an average kinetic energy of 4.3 eV are prepared in the top $F_2$/Ar layer of a stack.

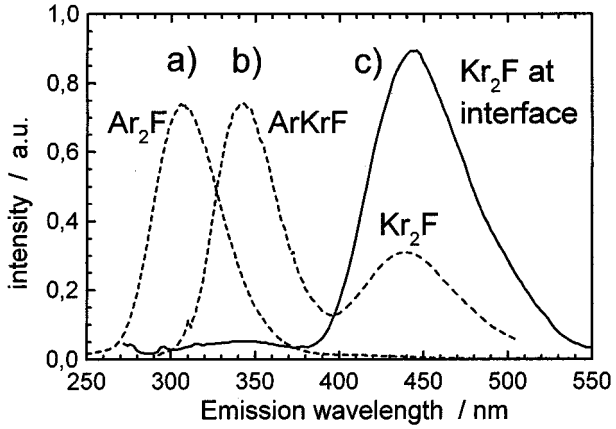


FIG. 3. Emission spectra of $Rg_2F$ exciplexes for different local surroundings of the F atom: (a) $Ar_2F$ band at 315 nm of an $F_2$ doped Ar matrix excited with 11.8 eV; (b) an ArKrF band at 345 nm and a $Kr_2F$ band at 439 nm of an Ar matrix doped with $F_2$ and Kr, also excited with 11.8 eV; (c) a $Kr_2F$ band at 444 nm of a standard stack excited with 10.15 eV (solid line).

### B. $Kr_2F$ emission of F atoms at the Kr/Ar interface

Electronic excitation of F atoms in rare gas matrices leads for sufficiently high energies to atomic F emissions, especially in Ne matrices.[26] For lower energies, exciplexes of fluorine with rare gas atoms are generated, and the emission of trimers prevails compared to dimers due to the lower energies[3,27] similar to the heavier halogens.[3] The emission energies of $Rg_2F$ trimers, formed with different rare gas atoms Rg, reflect the ionization energies of the rare gas atoms since charge transfer states are involved.[3,27] The variation of emission energies was used to distinguish between F atoms with different local environments, i.e., placed in different layers of the stack. This is illustrated in Fig. 3. Excitation of an Ar film, exclusively doped with $F_2$, in the Ar exciton band (11.8 eV) leads to one emission band [Fig. 3(a)] at 315 nm, which is characteristic for $Ar_2F$.[15,27] The same excitation energy, combined with an Ar film multiply doped with Kr and $F_2$, leads to a complete quenching of the $Ar_2F$ emission and the appearance of two new bands at 345 and 439 nm [Fig. 3(b)], which have been attributed to ArKrF and $Kr_2F$ trimers.[3,27] Changing the excitation energy to 10.15 eV as used for the photomobility experiments and irradiating a standard stack composed of Kr, covered with Ar and topped with $F_2$/Ar, yields only the $Kr_2F$ emission, but now slightly red shifted to 444 nm, as shown in Fig. 3(c). Obviously, only those F atoms that have reached the Kr film contribute to the emission spectrum, whereas F atoms, which remained in the Ar layers do not show up. Therefore the intensity at 444 nm can be taken as a sensitive measure for the number of F atoms that have penetrated the entire Ar layer. The small shift of 5 nm in wavelength of the $Kr_2F$ emission from Fig. 3(b) to Fig. 3(c) is significant and delivers additional information on the local environment of the F atoms, as is illustrated in Fig. 4. The center of the emission band shifts sys-

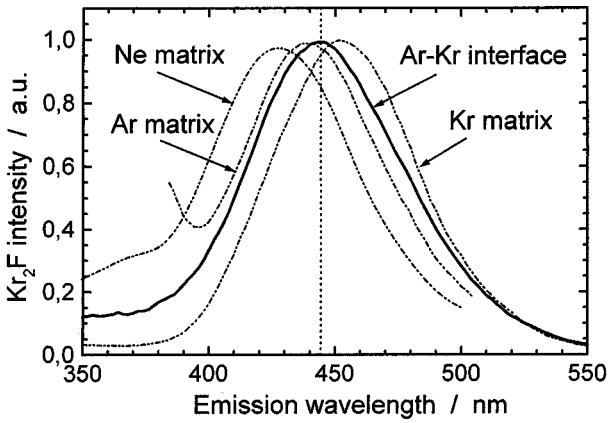


FIG. 4. $Kr_2F$ emission in different rare gas matrices. The bands (dotted lines) shift systematically to the red for $Kr_2F$ centers isolated in Ne (430 nm), Ar (439 nm), and Kr (453 nm) matrices, respectively. For a layered stack (solid line) the emission is situated at 444 nm, just in between the bands for Ar and Kr matrices.

tematically to the red for $Kr_2F$ centers isolated in Ne (430 nm), in Ar (439 nm), and in Kr matrices (453 nm). The band from the stack in Fig. 3(c) is situated just in between the emission bands for Ar and Kr matrices and is given by the solid line in Fig. 4. The shifts of the transition energies are assigned to a stepwise lowering of the $Kr_2F$ charge transfer state energies by an increase in polarizability of the matrix[3] from Ne to Kr. The local polarizability seen by the $Kr_2F$ centers formed in the stack seems to be half that of the Kr substrate and half that of the Ar spacer layer. This indicates that the F atoms remain predominantly in the Kr/Ar interface and are not injected into the Kr film.

The spectra in Fig. 3 demonstrate, in addition, that for the excitation energy of the photomobility experiments (10.15 eV) no $Ar_2F$ emission occurs. This is important because the small excess energy gained by the F atom on the repulsive $Ar_2F$ ground state surface can mobilize F atoms, as reported in Ref. 6, and could thus lead to an overestimation of the penetration depth. Such mobilization processes based on successive excitation of isolated F atoms in the Ar layers, and a subsequent $Ar_2F$ emission can be excluded according to Fig. 3. The reason is a small excitation probability of F atoms in Ar at this photon energy because the Ar matrix is still transparent, and the absorption bands of ArF are located at smaller photon energies.[27]

### C. Sensitivity increase by energy transfer from Kr excitons to F atoms

The accumulated density N of F atoms at the Kr/Ar interface has to be kept significantly below that of a monolayer ($6\times10^{14}$ F atoms per $cm^2$), because otherwise recombination to $F_2$ would occur, and an upper limit of 1/20th of a monolayer ($3\times10^{13}$ F atoms per $cm^2$) is derived in Sec. V B. Direct excitation of F atoms at the interface, for example in the $B\leftarrow X$ transition of KrF with a cross section of $\sigma=3.9\times10^{-19}$ $cm^2$ for a wavelength of 275 nm,[7] amounts to a maximal absorption probability $A=(1-\exp[-\sigma N])$ of only $A=1.2\times10^{-5}$.

The detection efficiency for fluorescence photons of $\eta=2\times10^{-6}$, resulting from an angular acceptance of $4.6\times10^{-3}$, a combined efficiency of monochromator and photomultiplier of $1\times10^{-2}$ and a ratio of $4\times10^{-2}$ for the monochromator to $Kr_2F$ bandwidth, together with the incident photon flux $I_0$ of typical $8\times10^{11}$ photons/s and the absorption probability $A$, would yield an upper limit of 20 counts/s for the count rate $I=\eta\cdot I_0\cdot A$. A decrease by one to two orders of magnitude to determine the penetration probability would be difficult to measure. The low absorption probability in the diluted F atoms of about $10^{-5}$ thus prohibits a sensitive detection. This limitation can be overcome by energy transfer of Kr excitons to the F atoms at the interface. Light that penetrates into the Kr film is completely absorbed close to the surface and generates excitons. These excitons are mobile, reach the surface with a high probability, and can transfer their energy to the F atoms, which will subsequently radiate. This process was previously addressed as quenching of rare gas excitons by adsorbates on the surface.[28] It can enhance the sensitivity by a factor of 800, allowing the detection of 1/1000th of a monolayer of F atoms, as will be shown below. The high absorption coefficient of about 0.2 $nm^{-1}$ in the Kr exciton band[29] at the photon energy of 10.15 eV corresponds to a light penetration depth in the Kr layer of about 5 nm, and essentially all photons entering the 30 nm thick Kr layer in a stack are absorbed while only 50% are lost due to the high reflectivity.[29] The Kr excitons are mobile[28] and in the $n=1$ exciton at 5 K diffusion lengths up to 100 nm have been determined.[28] The diffusion lengths exceed the light penetration depth considerably, and about half of the excitons will move toward the Kr/Ar interface and may transfer their energy[28] to the F atoms.

The highest observed count rates with the aforementioned sensitization reached values of 16 000 counts/s and demonstrate that the sensitivity was increased by a factor of 800, compared to direct excitation of the F atoms. The excitation probability per incident photon with sensitization corresponds to $10^{-2}$, which includes the estimated losses of 0.25 by reflectivity (0.5) and exciton directions (0.5). The energy transfer probability thus is of the order of $4\times10^{-2}$ for a coverage of 1/20th of a monolayer. This is consistent with a cross section for a transfer close to the size of a lattice atom. The maximal observed excitation probability remains significantly below unity, which is a precondition for a linear dependence of the $Kr_2F$ intensity on F concentration. Indeed, the signal decreased by a factor of 4 when the $F_2$ concentration was reduced from 2% to 0.5% for several spacer layer thicknesses. Signals of 200 counts/s can be reliably separated from the background. Since a signal of 16 000 counts/s corresponds to 1/20th of a monolayer, it has to be pointed out that the sensitivity was increased to less than 1/1000th of a monolayer of F atoms at the Kr/Ar interface. The excitation cross section of about $3\times10^{-16}$ $cm^2$, combined with the photon flux of $8\times10^{14}$ photons/$cm^2$ s, indicates that the F

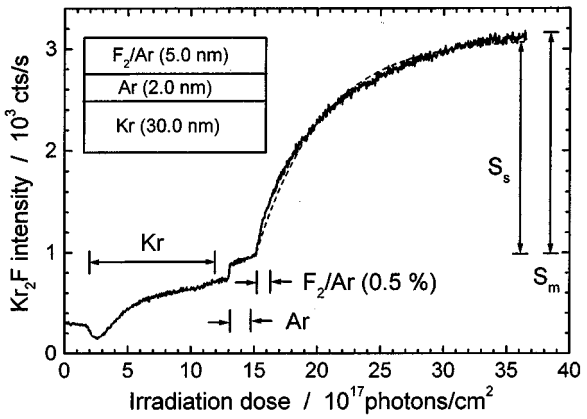


FIG. 5. The $Kr_2F$ intensity at 444 nm versus the irradiation dose ($h\nu = 10.15$ eV) during the deposition of a sample. Horizontal arrows show the deposition phases of the individual layers. $S_m$ is the experimental saturation value and the dashed line represents a fit by Eq. (2) with saturation value $S_s$.

atoms are excited about once per 4s (radiative lifetime $\approx 10^{-7}$ s).

## IV. PENETRATION DEPTH MEASUREMENTS

A typical sequence of layer depositions for a penetration depth measurement is depicted in Fig. 5. The sample was irradiated all the time with 10.15 eV photons and the accumulated dose is indicated on the abscissa while the emission intensity at the maximum of the $Kr_2F$ emission (444 nm) is shown on the ordinate. Here and in Fig. 7 the count rates were corrected for the slowly decreasing light flux due to the decay of the electron current in the storage ring. In the beginning, the bare $MgF_2$ substrate shows a background at 300 counts/s. The duration for condensation of the 30 nm thick Kr detection layer is indicated by a horizontal arrow in Fig. 5. The background intensity from the substrate diminishes first due to the higher reflectivity of the Kr film and increases later on to a background of about 800 counts/s due to energy transfer to the emitting color centers. The permanent irradiation guarantees that saturation is reached in this background, according to the growth curve in Fig. 5. A small stepwise increase to 900 counts/s is observed at the beginning of condensation of the Ar spacer layer, probably due to the change in reflectivity of the Kr/Ar sandwich (Fig. 2). The intermediate Ar layer in this sandwich is only 2 nm thick and is finished in the indicated short time interval.

The final $F_2$/Ar top layer (5 nm thickness) is condensed in a slightly shorter time interval (Fig. 5). A steep increase in intensity is observed with the beginning of the $F_2$/Ar condensation that continues for a long time after the condensation was finished. An increasing amount of $F_2$ is dissociated with the accumulated dose, part of the F atoms penetrate the Ar spacer layer and are enriched on the Kr/Ar interface, yielding emission spectra similar to that in Fig. 3(c). The $Kr_2F$ intensity smoothly saturates with a value $S_m$ of 2200 counts/s above the background for a dose of about $2 \times 10^{18}$ photons/cm$^2$ accumulated in the $F_2$/Ar film. The saturation value represents the maximal amount of F atoms that can be transferred to the Kr/Ar interface from the entire $F_2$ content on the top layer. Thus, $S_m$ is proportional to the probability that F atoms cross a given spacer layer, provided that stacks with top layers of the same composition and thickness are used. A series of stacks with different spacer layer thickness $d$ and as identical as possible top layers (0.5% $F_2$/Ar, 5 nm thick) and detection layers (Kr, 30 nm thick) was grown and irradiated. The collection of $S_m$ values in Fig. 6(a) clearly reflects the decreasing probability for penetrating the spacer layers with increasing thickness. Each point represents one stack, and for each stack a complete irradiation sequence similar to Fig. 5 was taken to determine the individual background and $S_m$ values. The error bars in Fig. 6(a) include the scattering in the background signal. To eliminate systematic errors, two independent sets of measurements were performed for which the position of the three condensation tubes was changed, and the calibration of the quartz balance was renewed. The two sets are distinguished by open and full squares in Fig. 6(b). They are quite compatible, and the penetration probability decreases exponentially within the reproducibility according to the semilogarithmic plot in Fig. 6(b). The penetration probability is reduced to 10% for a spacer thickness around 6 nm (23 Ar monolayers), and the sensitivity is sufficient to detect F atoms up to a thickness of 10 nm (38 Ar monolayers). The semilogarithmic plot suggests a thickness dependence,

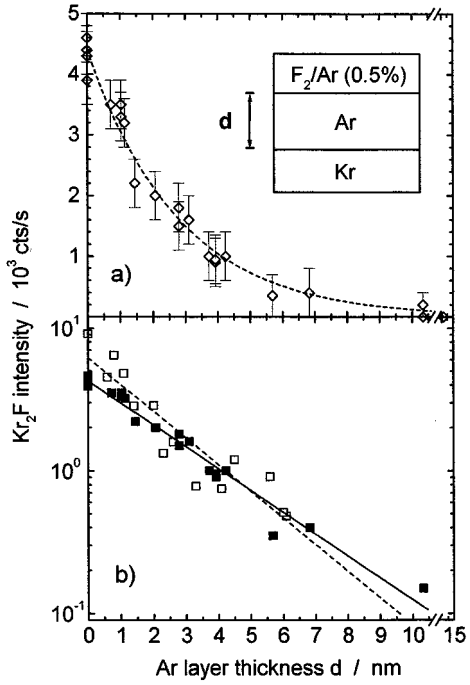


FIG. 6. Dependence of the saturation value $S_m$ (see Fig. 5) on the thickness $d$ of the intermediate Ar layer: (a) the first dataset on a linear scale; the exponential fit is included (dashed line). The error bars include the scattering in the background signal. (b) The first dataset (full squares) and second (open squares) dataset on a logarithmic scale. The solid and dashed lines are fits with Eq. (1) to the two sets with mean penetration depths $d_0$ of 2.8 and 2.3 nm, respectively.

$$I(d) = I_0 \exp(-d/d_0), \tag{1}$$

with a mean penetration depth $d_0$ of 2.8 nm for the first and of 2.3 nm for the second dataset, corresponding to an average of ten Ar monolayers.

In the attempted ideal case, an $F_2$ molecule is dissociated by one photon and an F atom is kicked by this single photon event to the Kr/Ar interface or gets permanently lost by trapping. The growth curve in Fig. 5 reflects the absorption cross section $\sigma_{F_2}$ (for $h\nu = 10.15$ eV) of the $F_2$ molecule times the dissociation probability $q$ and times the accumulated dose $D$ (photons/cm$^2$). The fluorescence intensity $I_F$ at 444 nm is proportional to the excitation intensity $I_E$ at 10.15 eV, and is given by

$$I_F = \eta \cdot I_E(1 - \exp[-\sigma_{F_2} \cdot q \cdot D]), \tag{2}$$

with a constant $\eta$ that reflects the light collection efficiency. A fit to the growth curve with Eq. (2) is shown in Fig. 5 and it delivers a value of $q \cdot \sigma_{F_2} = 2 \times 10^{-18}$ cm$^2$ according to the dose of $5 \times 10^{17}$ photons/cm$^2$ with a saturation intensity $S_s$ of 2100 counts/s. The experimental $S_m$ value at the end of the irradiation period is somewhat larger as $S_s$ and $S_m$ would softly increase further for longer irradiation times. This may be attributed to the dissociation of $F_2$ molecules that were formed by recombination of a previously trapped F atom with another mobilized F atom. The percentage of this overshoot is about the same within the reproducibility for all extensively irradiated stacks. Therefore the same average penetration depth of ten monolayers is obtained from the thickness dependence of $S_s$, and in the following only the $S_m$ values from Fig. 6 will be discussed. The $\sigma_{F_2} \cdot q$ values in the fits are rather sensitive to the immediate growth that is connected with the deposition of the of the $F_2$/Ar top layer (Fig. 5). During deposition, the accumulation of $F_2$ is superimposed on the dissociation history. This leads to a rather strong scatter in the $\sigma_{F_2} \cdot q$ values by a factor of 3 around the average value of about $4 \times 10^{-18}$ cm$^2$. A biexponential expression improves the quality of the fits, but the interpretation of the fitting parameters is not obvious and therefore it is not discussed here. The small cross section obtained for a dissociation efficiency close to unity, which is expected for the high kinetic energies,[13] is consistent with the weak absorption in the spin forbidden transition (Sec. III A).

A special behavior was observed for samples with $d = 0$, i.e. without Ar spacer layer, where the $F_2$/Ar top layer is in direct contact with the Kr layer. Figure 7(a) shows an irradiation sequence for such a sample. The indicated time interval for the top layer condensation is quite short. Nevertheless, a very fast rise during the condensation to about three-fourths of the final saturation intensity is observed. The further rise to the saturation plateau is significantly smoother. For $d = 0$ a certain amount of $F_2$ molecules will be condensed directly in the Kr/Ar interface, and these molecules can be responsible for the effect (see Sec. V B). Therefore the $F_2$ concentration was increased by a factor of 4 to 2% while the $F_2$/Ar layer thickness was reduced to 1 nm. Indeed, during the indicated short $F_2$/Ar condensation an extremely large and fast rise to 14 000 counts occurs [Fig. 7(b)], confirming a contribution by $F_2$ molecules at the interface. After completion of the top layer, a decrease in intensity, in contrast to the usual increase [Fig. 7(a), Fig. 5] is observed. Also, for the higher $F_2$ concentration this special behavior shows up exclusively in stacks without a spacer layer. The insert [Fig. 7(c)] shows the ordinary growth behavior for 2% of $F_2$ in the Ar top layer and a spacer layer of 3 nm thickness.

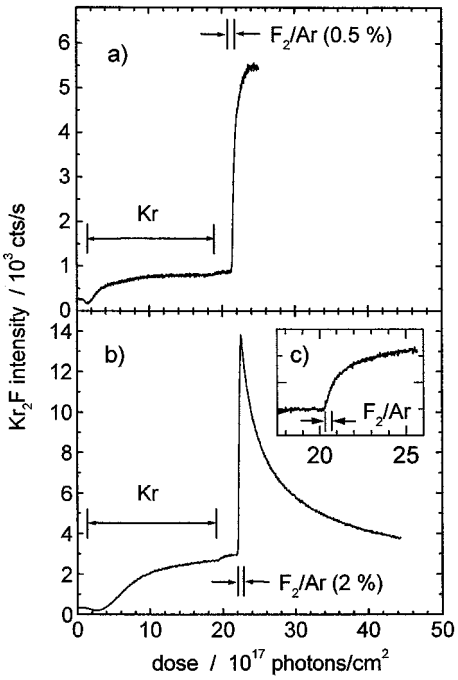


FIG. 7. $Kr_2F$ intensity at 444 nm, as in Fig. 5. (a) The sample with a 0.5% $F_2$ concentration, without an intermediate layer (60 nm Kr, 3 nm $F_2$/Ar); (b) the sample with a 2% $F_2$ concentration, without an intermediate layer (30 nm Kr, 1 nm $F_2$/Ar); (c) like (b), but with an intermediate Ar layer of 3 nm thickness.

## V. DISCUSSION

### A. Penetration depth

The penetration probabilities versus thickness, which are displayed in Fig. 6, follow an exponential with a scattering of about 10% for more than one order of magnitude of damping. This justifies the use of an exponential decay, and a mean penetration depth of $d_0 = 2.5$ nm $\pm 0.3$ nm or $10 \pm 1$ Ar monolayers is derived. The comparison with the modeling in Ref. 13 can only be qualitative because different kinetic energies are used. The modeling seems to predict an increase of the penetration depth with increasing kinetic energy. Four long range trajectories out of 50 were obtained for a kinetic energy of 2.8 eV. Our result corresponds to 18 trajectories out of 50 for a kinetic energy of 4.3 eV, and such an increase seems to be plausible, at least qualitatively. In this sense our results are consistent with this modeling. Calculations at higher energies with better statistics, and especially significantly larger clusters that can contain trajectories reaching up to 10 nm from the origin, would be required for a more quantitative comparison.

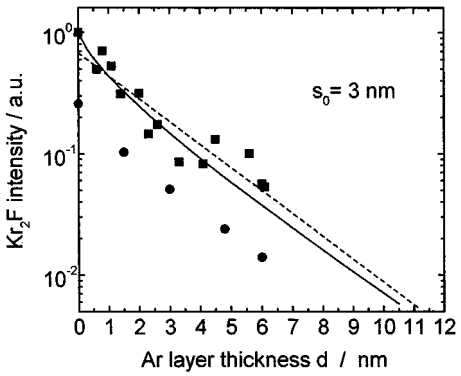


FIG. 8. The second dataset from Fig. 6 (full squares). A fit (solid line) assuming isotropical emission of the hot F atoms in the top layer, rectilinear trajectories, and an exponential damping yields an average length of travel of $s_0=3$ nm. Including the 5 nm thick top layers in the fit results in the circles. The dashed line shows the simple exponential fit [Eq. (1)].

The penetration probabilities of the neutral F atoms in Ar exceeds those observed for $F^+$ and $F^-$ ions through rare gas films[1] by orders of magnitude, since for $F^+$ and $F^-$ already one, respectively, three monolayers are sufficient to attenuate the transmission to $10^{-2}$. A stopping of the ions by closing channels in the rare gas lattice with the third layer in a face-centered cubic (fcc) structure was proposed. Obviously, such an effect is less effective for the neutral F atoms in the Ar lattice, and, on the contrary, our results are more consistent with the modeling,[13] which predicts long trajectories of nearly rectilinear motion through the channels of the lattice.

The ions in the attenuation experiments were collimated in a narrow cone vertical to the covering film due to the anisotropy of the $PF_3$ dissociation.[1] The F atoms in our case have no apparent preferential direction and are injected presumably isotropically from the $F_2$/Ar top layer into the Ar spacer layer. The F atoms in off-normal direction have a longer path to reach the Kr substrate, and thus the mean penetration depth determined in our experiment would be smaller than that derived for a directed beam. For a first estimate of this effect we assume rectilinear trajectories, F atoms that start isotropically at the top surface of the spacer layer, and an exponential damping. The integration of the angular distribution yields for very thin spacers a faster decay of the penetration probability versus $d$ compared to the single exponential [Eq. (1)]. F atoms starting rather parallel to the surface have initially a chance to penetrate, but they die out soon with increasing $d$ due to the very long real path to the Kr surface and due to the exponential damping. For larger $d$ values only atoms within a narrow cone normal to the surface survive and the further attenuation curve approaches the simple exponential. A fit to the experimental data, including the angular integration, is shown by the solid line in Fig. 8. It has the expected behavior and yields an average length of travel of $s_0=3$ nm. As expected, $s_0$ exceeds the penetration depth $d_0$, but the increase is only of the order of 10%–20%. The nonexponential part is only significant for very thin spacers and is lost in the scattering of the data points. In a second step, the F atom motion in the $F_2$/Ar top layer was also included. Thus, F atoms were started in the $F_2$/Ar top layer at different distances from the top of the Ar spacer layer. Integration over the top layer thickness of 5 nm with isotropic angular distribution yields, for rectilinear trajectories and an average length of travel $s_0$ of 3 nm the circles in Fig. 8. The $d=0$ value is lower due to F atom trapping in the top layer. The decrease with thickness after normalization to the $d=0$ value is again consistent with the experimental data, which demonstrates that the determined penetration depths are not sensitive to the used $F_2$/Ar layer thickness. For comparison, the simple exponential fit is included in Fig. 8 (dashed line).

A larger average length of travel values $s_0$ for a measured penetration depth $d_0$ will be obtained if several large angle scattering events have to be included. They will lead in the extreme case to an isotropic diffusive Brownian-like motion. The mean displacement $\overline{x^2}$ is closely related to $d_0^2$ and is given by the mean-free path $l$ for large angle scattering events, together with the number $K$ of jumps in statistical directions,

$$d_0^2=K\cdot l^2 \quad \text{and} \quad s_0=K\cdot l. \tag{3}$$

A lower limit of $l$ is given by the nearest neighbor separation of Ar (0.38 nm). Using the experimental value $d_0=2.5$ nm leads to $K=44$ and to an upper limit of $s_0<17$ nm. This $K$ value is unreasonably high since for a large angle scattering event, the energy loss $\Delta E$ per head-on collision for an atom with energy $E$ corresponds to $\Delta E/E=4m_1m_2/(m_1+m_2)^2$ and the loss averaged over the scattering angle[30] is $\overline{/\Delta E/E/}=1/2\Delta E/E$. Thus, for the atomic masses of F($m_1=19$ amu) and Ar($m_2=40$ amu) the average energy loss $\overline{/\Delta E/E/}=0.44$ per collision. The initial kinetic energy of an F atom of 4.3 eV will be reduced below 0.3 eV after five collisions and below 0.1 eV after seven collisions. Only one cage exit out of 100 trajectories was found in the molecular dynamics simulation for kinetic energies of 0.07 to 0.12 eV,[14] and for a diffusive motion F atoms are expected to come at rest for $K\leqslant 7$. Thus, a mean-free path $l$ for large angle scattering events of $l\geqslant 0.9$ nm and an $s_0\leqslant 7$ nm is derived. This realistic estimate for a diffusive motion leads to an average length of travel $s_0$, which exceeds the penetration depth by about a factor of 2. With $l\geqslant 0.9$ nm it suggests, similar to the simulation,[14] that, on average, at least three monolayers are crossed without an appreciable change in direction and without energy loss.

A comparison with the available experimental data for the range of neutral F atoms is again hampered by the different kinetic energies. For the cage exit after radiative decay of $Ar_2$ F centers an average length of travel of $s_0=7$ nm was derived.[6] The molecular dynamics modeling attributed only a kinetic energy of 0.07–0.12 eV to the F atoms in this case, with only two cage exits to the next lattice site for 300 trajectories and none of the longer range.[14] Even if the diffusive limit with $s_0\leqslant 7$ nm is accepted for the F atoms with 4.3 eV energy, we would expect at the low kinetic energies in the $F_2$/Ar experiment in combination with the trends in the simulation[13,14] an $s_0$ value smaller than 7 nm. Presumably,

the averaging on the F-F spatial distributions[6] caused an overestimate in $s_0$. In the shuttling experiments $s_0 \approx 4$ nm (ten lattice sites) was estimated for kinetic energies of 0.5 eV.[7] This value can be consistent with the diffusive limit.

### B. Processes at the Kr/Ar interface

A comparison of Fig. 5 and Fig. 7 demonstrates that processes with two different species, i.e. F atoms and $F_2$ molecules, have to be considered. The F atoms contribute in all stacks and lead to an intensity rise due to the increasing amount of fragments. $F_2$ molecules are active only in stacks without spacer layer and the intensity emitted in processes related to them decreases with irradiation due to their dissociation. In this case the increase from accumulating F atoms competing with the decrease from $F_2$ can produce a complicated irradiation dependence, and therefore the F atom case is discussed first. A top layer of 0.5% $F_2$ in Ar with a thickness of 5 nm, as used for a standard stack, contains an amount of $F_2$ similar to one-tenth of a monolayer and delivers a maximal signal of 4000 counts/s. Only 25% of them or 1/40th of a monolayer reaches the interface if angle integration and the $d_0$ of 2.5 nm are taken into account. The intensity did not exceed 16 000 counts/s, even for a $F_2$ content, increased by much more than a factor of 4, demonstrating that also in these cases the amount of F atoms at the interface remained below one-tenth of an isolated monolayer, obviously due to clustering effects. The limiting value of one-tenth of a monolayer is plausible for the case of 12 nearest neighbors in a fcc lattice. The sensitization by energy transfer from Kr excitons determines the high sensitivity according to Sec. III C. Energy transfer by free and by self-trapped excitons has to be considered. Free excitons are created close to the interface and reach it with a high probability due to the large diffusion length.[28] The exciton energy is just resonant with excited states of Kr atoms in the lattice and neutral KrF excitations can switch without barriers via curve crossing to the ionic $Kr^+F^-$ surfaces and finally form the lower lying $Kr_2^+F^-$ exciplexes. The transfer cross section is close to the size of a lattice atom (Sec. III C) and also comparable with the size of an $n=1$ exciton. Thus, a collisional type of energy transfer by a free exciton to an F atom is consistent with this picture. Self-trapped excitons in the Kr film could transfer energy in principle by dipole–dipole interaction[28] with a rate that decreases with the sixth power of the distance. Integration over the spatial distribution of self-trapped excitons and of F atoms[28] would lead to a progressive increase of sensitivity with F atom concentration, which is in contradiction to the linear concentration dependence observed up to 2% of $F_2$. Also, F atoms in the spacer layer could come into play up to distances comparable with the Förster Dexter radius.[31] This disagrees with the $Kr_2F$ emission spectra that are dominated by F atoms in the interface (see Fig. 3). The self-trapped excitons with an energy of 8.4 eV are lower in energy by 1.7 eV than the excitons, and the Förster Dexter radius is small because resonant KrF states are not available at this energy.

Next, the $F_2$ contribution is treated, and it might be surprising that it appears so strongly in the $Kr_2F$ emission (Fig. 7). $F_2$ molecules, condensed at the interface during preparation of an $F_2$/Ar layer without a separating Ar spacer, can be excited by free Kr excitons similar to the F atoms. The energy is sufficient to form $Kr^+(F_2)^-$ charge transfer states and via the harpooning mechanism $Kr^+F^-F$ configurations eject an F atom[3] and an excited $Kr^+F^-$ exciplex remains in the interface. The $Kr^+F^-$ exciplexes relax further to $Kr_2^+F^-$ centers that decay radiatively by emission of the typical $Kr_2F$ emission. In this way $F_2$ dissociation at the interface leads to the characteristic emission that appears also for F atoms transported to the interface. The $F_2$ content is maximal just at the beginning of the irradiation and produces the prompt rise in Fig. 7(a) to about three-fourths of the saturation value. The $F_2$ content decreases due to the dissociation that is responsible for the signal and dies out for long irradiation times [Fig. 7(a)], provided the concentration in the interface is low enough to prevent recombination.

The F atom concentration at the Kr/Ar interface increases due to the accumulation of penetrating atoms, and in the saturation value only this part survives. Therefore, also the saturation value of stacks without Ar spacer fit smoothly in the thickness dependences (Fig. 6). For the higher $F_2$ concentration in Fig. 7(b), the decrease by $F_2$ dissociation is so strong that it is not compensated by the increasing F atom contribution, and the saturation value is lower than expected. The 2% concentration corresponds to about 1/50th of an $F_2$ monolayer at the interface from the condensation and up to 0.5 monolayers from the content in the entire film. The high content can lead to $F_2$ clusters by subsequent dissociation and recombination events. In $F_2$ clusters, like in pure $F_2$ films, the $Kr_2F$ emission is quenched, which explains the low intensities at long irradiation times. Trapping in a spacer layer reduces the final amount of F atoms at the interface considerably and the ordinary behavior is observed for stacks with spacers [Fig. 7(c)]. Perhaps also self-trapped excitons in the Kr film excite $F_2$ molecules at the interface by dipole–dipole energy transfer in contrast to the F atom case. It would enhance the prompt rise, especially for higher $F_2$ concentrations. If there is energy transfer by dipole–dipole interaction to $F_2$ molecules in the Ar films (with or without Ar spacer), it will speed up the $F_2$ dissociation since it adds to the dissociation by photons. Energy transfer can be active only close to the Kr surface and transfer to $F_2$ does not influence the determined penetration depths since the saturation values are not changed, but only the rates.

## VI. CONCLUSIONS

Obviously, the sandwich experiment yields a well-defined large penetration depth of $d_0 = 2.5$ nm or ten monolayers for neutral F atoms, which poses an interesting question why the attenuation is so much larger for ions.[1] A conversion to an average length of travel $s_0$ with respect to the experiments in doped samples depends on the type of motion. $s_0$ exceeds $d_0$ only moderately for a rectilinear motion that is supported by simulations. Diffusive motion that was presumably anticipated in the evaluation of the doping

experiments can lead to $s_0 \leqslant 7$ nm for the measured $d_0$. The method of F atom detection is very effective and even an F atom density of 1/1000th of a monolayer at the Kr/Ar interface can be recorded reliably. In the sandwich samples the dissociation and cage exit processes are spatially well separated from the final location of the investigated F atoms. By introducing a further film of molecules that react with the F atoms, it will be possible in future experiments to study the bond formation as a well-defined final step in addition to cage exit and transport.

## ACKNOWLEDGMENTS

The valuable contributions of J. Kuder in the early stages of the experiment are gratefully acknowledged. This work was supported by the BMBF via Contract No. 05/5KEAYB5 and by the Deutsche Forschungsgemeinschaft via Schw230/10-1.

[1] N. J. Sack, M. Akbulut, T. E. Madey, P. Klein, H. M. Urbassek, and M. Vicanek, Phys. Rev. B **54**, 5130 (1996); T. E. Madey, N. J. Sack, and M. Akbulut, Nucl. Instrum. Methods Phys. Res. B **100**, 309 (1995); M. Akbulut, N. J. Sack, and T. E. Madey, Phys. Rev. Lett. **75**, 3414 (1995).
[2] M. Chergui and N. Schwentner, *Trends in Chemical Physics*, edited by J. Menon, Trivandum India Vol. 2, 89 (1992); J. Zoval and V. A. Apkarian, J. Phys. Chem. **98**, 7945 (1994).
[3] M. E. Fajardo and V. A. Apkarian, J. Chem. Phys. **85**, 5660 (1986); M. E. Fajardo and V. A. Apkarian, *ibid.* **89**, 4102 (1988); M. E. Fajardo, R. Withnall, J. Feld, F. Okada, W. Lawrence, L. Wiedemann, and V. A. Apkarian, Laser Chem. **9**, 1 (1988).
[4] G. Zerza, G. Sliwinski, and N. Schwentner, Appl. Phys. B: Photophys. Laser Chem. **55**, 331 (1992); G. Sliwinski and N. Schwentner, SPIE Proc. 3052, edited by F. A. Atanasov, Bellingham, 1996, p. 23.
[5] N. Schwentner and V. A. Apkarian, Chem. Phys. Lett. **154**, 413 (1989).
[6] J. Feld, H. Kunttu, and V. A. Apkarian, J. Chem. Phys. **93**, 1009 (1990).
[7] H. Kunttu, J. Feld, R. Alimi, A. Becker, and V. A. Apkarian, J. Chem. Phys. **92**, 4856 (1990).
[8] H. Kunttu, E. Sekreta, and V. A. Apkarian, J. Chem. Phys. **94**, 7819 (1991).
[9] K. Gödderz and N. Schwentner, Low Temp. Phys. **22**, 157 (1996).
[10] E. Y. Misochko, V. A. Benderskii, A. U. Goldschleger, A. V. Akimov, and A. F. Shestakov, J. Am. Chem. Soc. **117**, 11 997 (1995).
[11] G. Zerza, F. Knopp, R. Kometer, G. Sliwinski, and N. Schwentner, SPIE Proc. 1410, 202 (1991).
[12] C. Bressler and N. Schwentner, Phys. Rev. Lett. **76**, 648 (1996).
[13] R. Alimi, R. B. Gerber, and V. A. Apkarian, J. Chem. Phys. **92**, 3551 (1990).
[14] I. H. Gersonde, Ph.D. thesis, Freie Universität, Berlin, 1992.
[15] H. Kunttu and V. A. Apkarian, Chem. Phys. Lett. **171**, 423 (1990).
[16] R. Alimi, R. B. Gerber, and V. A. Apkarian, Phys. Rev. Lett. **66**, 1295 (1991).
[17] A. I. Krylov and R. B. Gerber, Chem. Phys. Lett. **231**, 395 (1994).
[18] K. S. Kizer and V. A. Apkarian, J. Chem. Phys. **103**, 4945 (1995).
[19] J. Bahrdt, P. Gürtler, and N. Schwentner, J. Chem. Phys. **86**, 6108 (1987).
[20] N. Schwentner, E.-E. Koch, and J. Jortner, *Electronic Excitations in Condensed Rare Gases*, Springer Tracts in Modern Physics, 1985, Vol. 107, Chaps. 3,6.
[21] V. Saile, M. Skibowski, W. Steinmann, P. Gürtler, E. E. Koch, and A. Kozevnikov, Phys. Rev. Lett. **37**, 305 (1976).
[22] C. Bressler, W. G. Lawrence, and N. Schwentner, J. Chem. Phys. **105**, 1318 (1996).
[23] D. C. Cartwright and P. J. Hay, Chem. Phys. **114**, 305 (1987).
[24] H. Kunz, J. G. McCaffrey, R. Schriever, and N. Schwentner, J. Chem. Phys. **98**, 1039 (1991).
[25] E. A. Colbourn, M. Dagenais, A. E. Douglas, and J. W. Raymonda, Can. J. Phys. **54**, 1343 (1975).
[26] C. Bressler, W. G. Lawrence, and N. Schwentner, J. Chem. Phys. **102**, 48 (1995).
[27] C. Bressler, W. G. Lawrence, and N. Schwentner, J. Chem. Phys. **105**, 10 178 (1996).
[28] N. Schwentner, G. Martens, and H. W. Rudolf, Phys. Status Solidi B **106**, 183 (1981); B. Herkert, A. Schrimpf, K. Göttsche, T. Bornemann, R. Brüning, and H.-J. Stöckmann, Phys. Rev. B **51**, 15 763 (1995); G. Zimmerer, *Creation, Motion and Decay of Excitons in Rare Gas Solids*, Excited State Spectroscopy in Solids (Soc. Italiana di Fisica, Bologna, 1987), Vol. XCVI.
[29] I. T. Steinberger, P. Maaskant, and S. E. Webber, J. Chem. Phys. **66**, 4722 (1977).
[30] E. T. Tarasova, A. M. Ratner, V. M. Stepanenko, I. Ya. Fugol, M. Chergui, R. Schriever, and N. Schwentner, J. Chem. Phys. **98**, 7786 (1993).
[31] T. Förster, J. Chem. Phys. **2**, 55 (1948); D. L. Dexter, J. Chem. Phys. **21**, 836 (1953).